^{145}Ba β^- decay: Excited states and half-lives in neutron-rich ^{145}La

M. A. Cardona[1,2,3,*] D. Hojman,[1,2] B. Roussière,[4] I. Deloncle[4] N. Barré-Boscher,[4] M. Cheikh Mhamed,[4] E. Cottereau,[4] B. I. Dimitrov[5] G. Tz. Gavrilov,[5] A. Gottardo,[4,†] C. Lau,[4] S. Roccia,[4,‡] S. Tusseau-Nenez,[4,§] D. Verney[4] and M. S. Yavahchova[5]

[1]*Departamento de Física, Comisión Nacional de Energía Atómica, BKNA1650 San Martín, Argentina*
[2]*CONICET, C1033AAJ Buenos Aires, Argentina*
[3]*Escuela de Ciencia y Tecnología, Universidad de San Martín, BKNA1650 San Martín, Argentina*
[4]*Laboratoire de Physique des Deux Infinis Irène Joliot-Curie, CNRS/IN2P3 UMR 9012-Université Paris Saclay, F-91406 Orsay Cedex, France*
[5]*Institute for Nuclear Research and Nuclear Energy, Bulgarian Academy of Sciences, 1784 Sofia, Bulgaria*

Background: Neutron-rich nuclei in the A ≈ 140–160 mass region provide valuable information on nuclear structure such as quadrupole- and octupole-shape coexistence and the evolution of the collectivity. These nuclei have also a nuclear engineering interest because they contribute to the total decay heat after a fission burst. The information concerning ^{145}La is very limited.

Purpose: The study of low-spin states in ^{145}La will provide a more detailed level scheme and enable the determination of the half-lives of the excited states.

Methods: Low-spin excited states in ^{145}La have been investigated from the ^{145}Ba β^- decay. The ^{145}Ba nuclei were directly produced by photofission in the ALTO facility or obtained from the β^- decay of ^{145}Cs also produced by photofission. Gamma spectroscopy and fast-timing techniques were used.

Results: A new level scheme was proposed including 67 excited levels up to about 3 MeV and 164 transitions. Half-lives in the few-nanosecond range were measured for the first excited states. Configurations for levels up to ≈600 keV were discussed.

Conclusions: The available information on the low-spin states of ^{145}La has been modified and considerably extended. The analysis of the properties of the first excited states, such as excitation energies, decay modes, log ft values, reduced transition probabilities, and Weisskopf hindrance factors, has enabled the identification of the first members of the bands corresponding to the $g_{7/2}$, $d_{5/2}$, and $h_{11/2}$ proton configurations.

I. INTRODUCTION

Nuclei belonging to the neutron-rich $A \approx 140$–160 mass region, apart from developing quadrupole deformations, also have been suggested [1,2] to possess reflection asymmetric shapes. Large quadrupole deformations up to $\beta \approx 0.34$ have been observed in Sm isotopes [3]. In addition, octupole effects have been found in several nuclei like ^{145,147}La [4,5], bringing important information about quadrupole- and octupole-shape coexistence. In this region, the influence of the valence p-n in-

teractions in the evolution of the collectivity has been pointed out by Casten *et al.* [6]. For $N > 90$, the subshell $Z = 64$ disappears, resulting in a rapid development of the collectivity. This is related to the filling of highly overlapping proton and neutron orbitals, which have large p-n interactions, and hence constitutes the essential driving force to deformation. This region has also a nuclear engineering interest. Nuclei in this region contribute to the total decay heat after a fission burst and are relevant in the decay heat calculations [7]. Hence, their decay studies are important as a complement of the total absorption gamma spectroscopy studies. Therefore, an important effort was made to investigate the nuclear structure of neutron-rich nuclei around mass $A = 150$. Among these investigations, high-spin states were studied from the spontaneous fission of ^{252}Cf sources using multidetector arrays like Gammasphere [8,9], isomeric states by bombarding ^{239}Pu and ^{235}U targets with thermal neutrons [10,11], and low-spin states were studied through β^- decay from fission products obtained by bombarding UC$_x$ targets with protons [12] or electrons (inducing photofission) [13]. In this context, a research program

---

*cardona@tandar.cnea.gov.ar

†Present Address: Istituto Nazionale di Fisica Nucleare, Laboratori Nazionali di Legnaro, Viale dell'Università, 2, I-35020 Legnaro, Italy.

‡Present Address: Institut Laue-Langevin, 71 avenue des Martyrs, F-38042 Grenoble Cedex 9, France.

§Present Address: Laboratoire de Physique de la Matière Condensée, CNRS, Ecole Polytechnique UMR 7643-IP Paris-Route de Saclay, F-91128 Palaiseau Cedex, France.

has started at the Institut de Physique Nucléaire d'Orsay, France, to study neutron-rich nuclei with mass $A = 140$–170 produced by photofission followed by β^- decays using γ, β, and fast-timing spectroscopy techniques. We present here the results of our work concerning the ^{145}La nucleus. From investigations previous to this work, the decay of ^{145}Ba to ^{145}La has not been established completely and many γ rays remain unplaced or have been placed tentatively in the level scheme [14]. Moreover, except for the 2566 keV level (2570 keV in the present work), the available information on levels above 1177 keV concerns the population of pseudolevels based on total γ-ray absorption spectrometer measurements [15]. In addition, Shima *et al.* [16] are working on the excited states of ^{145}La nucleus populated through ^{145}Ba β^- decay using a 4π Clover detector.

II. EXPERIMENTAL PROCEDURE

The experiments were carried out at the ALTO-PARRNe facility at the Institut de Physique Nucléaire d'Orsay, France [17]. ^{145}La nuclei were obtained through the ^{145}Cs $\rightarrow$ ^{145}Ba $\rightarrow$ ^{145}La and ^{145}Ba $\rightarrow$ ^{145}La β^- decays, the Cs and Ba elements being produced by photofission. The linac accelerator ALTO provides a 50 MeV, 10 μA electron beam which hits a thick uranium-carbide (UC$_x$) target producing bremsstrahlung radiations that induce the fission of ^{238}U. The fission products released from the target effuse into a MK5 ISOLDE-type [18] hot plasma ion source via the transfer line. The temperature of the target and of the transfer line was 1950°C, that of the ion source 1800°C. The produced ions were extracted under 30 kV then mass-separated by the PARRNe uniform-field H-shaped magnet with a 65° deflecting angle and a mass resolving power of 1300. The radioactive ions were guided toward the BEDO measurement station [19] and implanted onto the Al-coated mylar tape of a moving tape collector. The measurement cycles were chosen to optimize the counting rate corresponding to the ^{145}Ba $\rightarrow$ ^{145}La decay: the collection (tc), waiting (tw), and measuring (tm) times were equal to tc = 4 s, tw = 2 s, and tm = 4 s. The detector setup consisted of two coaxial 70% Ge(HP) tapered EUROGAM-1-type detectors, one planar Ge(HP) detector, two LaBr$_3$(Ce) scintillator detectors, and a Pilot U plastic scintillator β detector placed in a close geometry surrounding the implanted source. The three Ge(HP) and the two LaBr$_3$(Ce) detectors were placed in the same plane, perpendicular to the radioactive ion beam at the collection point on the tape, while the β detector was placed along the beam line (Fig. 1). The scintillators were used for the fast-timing measurements [13,20]. One of the LaBr$_3$(Ce) detectors has a crystal of cylindrical shape of 25.4-mm diameter and 30-mm length and is coupled to a Hamamatsu H10570 photo-multiplier tube (PMT) assembly which incorporates the R9779 high speed PMT. The other LaBr$_3$(Ce) detector has a truncated conical shape with 25.4- and 38.1-mm front and back diameters and 38.1-mm length and is coupled to a Photonis XP20D0 PMT. For having a timing response almost independent of the β energy we used a thin plastic scintillator disk of 25.4-mm diameter and 3-mm
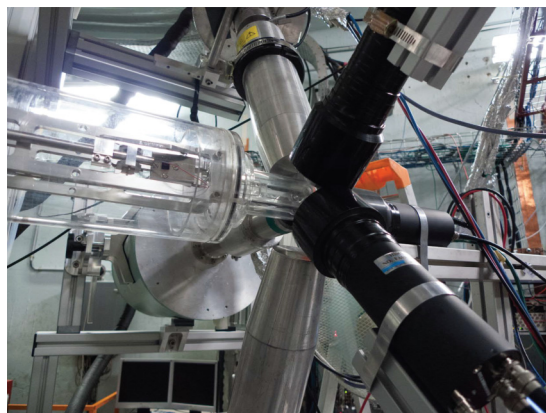

FIG. 1. Detector array at the BEDO measurement station. The radioactive ions are coming from the left, the β detector is placed behind the implanted source and the other detectors are mounted around the source in the plane perpendicular to the beam direction.

length coupled to a Hamamatsu H10570 PMT assembly. The last dynode outputs of the PMTs were processed by Ortec 113 preamplifiers and sent to amplifiers to provide the energy of the incident radiations. The anode signals fed the ORTEC 935 constant fraction discriminators (CFD). The CFD outputs provided the start or stop signals to three time to amplitude converters (TAC). The TACs were used for measuring the time difference between each pair of scintillators in the 50-ns range. The energy signals from the six detectors and the outputs of the three TACs were collected and processed using two COMET-6X modules associated with the NARVAL acquisition system [21], which recorded each signal with its absolute time (400-ps time resolution). This time resolution is not appropriate for fast-timing measurements, being the reason for the use of TACs. Coincidence events involving different detectors and/or TACs were constructed off-line and sorted in two- and three-dimensional matrices with different time coincidence windows, or energy-depending time ranges. The experiment was performed during 50 h. As examples of the statistics resulting from this work: 36 million double coincidence events between the two coaxial Ge(HP) detectors and 5 million double coincidence events between the two LaBr$_3$(Ce) detectors with the corresponding TAC were obtained fixing a coincidence time range of 1 μs. Obtaining accurate and reliable results from fast-timing measurements require great care, not only in the implementation of the experimental setup but also in the data analysis. The specific precautions taken in both domains have been described in Ref. [13]. The fast-timing electronic was adjusted using a ^{60}Co calibration source. Then, the performance and the time calibration of the fast-timing setup were checked in an online experiment through the measurement of the ^{138}Cs $\rightarrow$ ^{138}Ba decay. To this aim the mass-separator was set on $A = 138$ and the beam was guided and implanted onto the mylar tape during 10 s and set off while the accumulated radioactive sources were measured for the following 1800 s. This cycle time was chosen to optimize the counting rate corresponding to the ^{138}Cs $\rightarrow$ ^{138}Ba decay and was repeated during 14 h. Before collecting the data on $A = 138$ and 145, the yields of
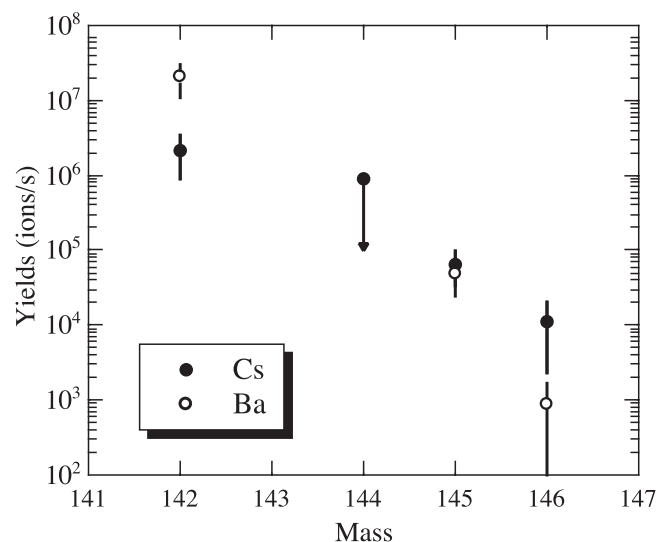
FIG. 2. Yields of Cs and Ba isotopes released by a UC$_x$ target heated to 1950°C and bombarded by a 50 MeV 10 μA electron beam.

nuclei with mass number close to 145 were estimated. The isotopes collected on the tape were identified by the characteristic γ-ray energies detected using one Ge(HP) detector, whose absolute efficiency was measured previously. The measuring time (tm from 2 to 10 s) was selected based on the half-lives of the elements of the given radioactive chain. The collection time (tc from 0.2 to 2 s) was adjusted to provide counting rates acceptable by the Ge(HP) detector.

III. EXPERIMENTAL RESULTS

Figure 2 displays the Cs and Ba yields measured, i.e., the radioactive ion beam intensity delivered by ALTO for a 10 μA electron incident beam. Yields of Xe could not be evaluated since, for $A = 144$, 145, and 146, the γ rays associated to the Xe $\to$ Cs decay or, for $A = 142$, their absolute intensities are not known. The absolute intensities of the transitions following the ¹⁴⁴Cs decay are not known [22], thus the ¹⁴⁴Cs yield was estimated from the number of ¹⁴⁴Ba $\to$ ¹⁴⁴La disintegrations observed and the value plotted in Fig. 2 is an upper limit.

Figure 3 shows the Ge(HP) γ-ray projection of the β-γ coincidence matrix, accumulated over the $A = 145$ experiment, where the main transitions are labeled. The strongest transitions correspond to the ¹⁴⁵Ba $\to$ ¹⁴⁵La decay. Nevertheless, the transitions corresponding to $A = 145$ long-lived nuclei are more intense than expected according to the selected measurement cycle. This fact could be due to an imperfect focus of the beam into the Al-coated mylar tape and hence a small amount of nuclei could be implanted out of the tape and consequently not evacuated from the measurement station after the measuring times. In Fig. 3, the presence of transitions belonging to the ¹²⁶In $\to$ ¹²⁶Sn decay is probably due to the extraction from the target of molecules including ¹⁹F and nuclei with $A = 126$. Indeed, prior to the present experiment, a small amount of CF4 was injected in the target ion source system and remained as contamination. No other influence of the CF4 has been detected.
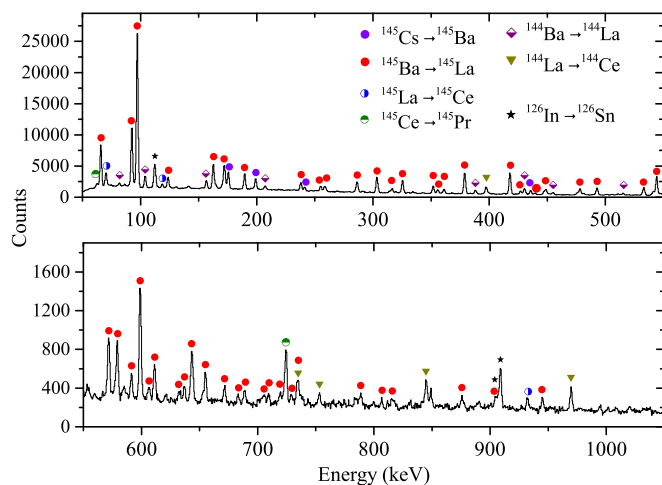

FIG. 3. Ge(HP) γ-ray projection of the β-γ coincidence matrix. The main transitions are labeled.

Figure 4 displays decay curves of γ rays from the $A = 145$ activity. In Fig. 4(a) the curves were normalized to 1000 at time $t = 0$. To improve the readability of Fig. 4(b), the curves were shifted by multiplying the values by arbitrary constants. This figure shows very similar decay curves for several strong transitions, confirming their assignments to the ¹⁴⁵Ba $\to$ ¹⁴⁵La decay.
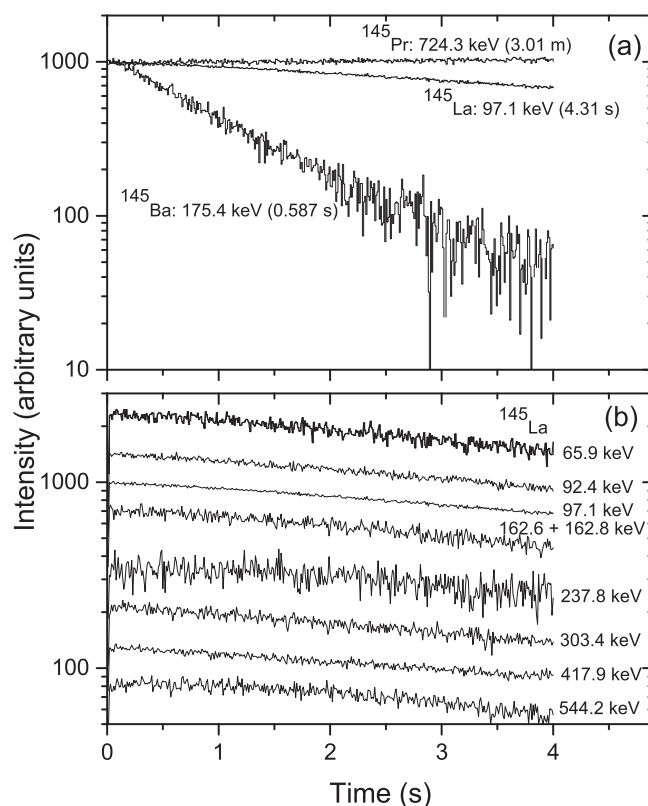

FIG. 4. Decay curves for: (a) selected transitions belonging to nuclei with $A = 145$, where the adopted half-lives of the corresponding parent nuclei [14] are indicated, (b) selected transitions assigned to ¹⁴⁵La.

The proposed level scheme for ^{145}La deduced in the present work is shown in two parts in Figs. 5 and 6, where previously reported transitions, levels, spins, and parities are drawn in red. The drawing of the level scheme was created using the ENSDAT code available at the Brookhaven National Laboratory website [24]. The assignment of transitions belonging to ^{145}La was based on coincidences with La X-rays and other transitions assigned previously to this nucleus, the knowledge of the neighboring $A = 145$ nuclei [14], and the decay curves for the strongest transitions. The level scheme consists of 67 excited levels up to about 3 MeV in energy and 164 transitions. Previous to this work low-spin states in ^{145}La populated through β^- decay of ^{145}Ba were reported mainly by Pfeiffer *et al.* [25]. In addition, high-spin states of ^{145}La nuclei produced in the spontaneous fission of ^{248}Cm and ^{252}Cf were studied by Urban *et al.* [4] and Zhu *et al.* [5]. Regarding the β^- decay work of Pfeiffer *et al.*, we confirmed all the transitions depopulating excited states with $E < 640$ keV, except the 247.5 keV line, while the remaining transitions have not been observed or have been placed elsewhere in the level scheme. We also confirmed the first three dipole and two quadrupole transitions of the ground state band [4,5] and the 334.3 keV E1 transition feeding this band. Our results do not support the existence of the 192.0 keV E1 transition reported in Ref. [5], but not retained in the adopted-γ list by evaluators [14]. None of the levels proposed in Ref. [14], above 750 keV, except the 2566 keV level, was confirmed in our work. The coincidence relationships have allowed us to establish the existence of 53 new excited levels. The 709.3, 719.4, 1693.4, 2311.6, and 2569.6 keV lines have been observed in singles and β-gated spectra but not in γ-γ coincidence spectra. They have been placed in the level scheme feeding the ground state since their energies match the corresponding level energies. The present extended level scheme can be used to improve the decay heat calculations after a fission burst [7].

Table I shows the adopted levels and transitions of ^{145}La. The γ-ray intensities were extracted from singles spectra except for some transitions located in complex parts of the spectra. For these transitions coincidence spectra between the two coaxial Ge(HP) detectors were used. Since the angle between the coaxial Ge(HP) detectors was 130° and they were placed in a close geometry, we neglected the influence of angular correlations. The β^--branching intensities have been calculated from total intensity imbalances, differing from the values measured with a total absorption γ-ray spectrometer (TAGS) [15]. In the present work only the 26% of the β^- decays is seen to feed levels above 1.2 MeV, while the measurements with TAGS indicate 68%. This disagreement is generally observed in high Q value β-decays where the density of states is important, decaying through a large number of transitions, many of them unobserved. In addition, we did not considered the direct feeding to the ground state. Nevertheless, the total β^--branching intensity to the ground and 65.9 keV states reported in Ref. [15] and our value for the 65.9 level suggest a small feeding to the ground state. In this context, β^--branching intensities and the corresponding log ft values reported in Table I must be assumed as upper and lower limits, respectively. Log ft values were calculated using the LOGFT code available at the Brookhaven National Lab-

TABLE I. Initial-level energy, β^--branching intensity, log ft, γ-ray energy, final-level energy, and γ-ray intensity of transitions of ^{145}La. I_β (log ft) must be assumed as upper (lower) limits (see text).

E_i (keV)	I_β (%)	Log ft	E_γ (keV)	E_f (keV)	I_γ
65.9	6.3(13)	6.33(10)	65.9	0	309(12)
97.1	5.3(12)	6.32(9)	97.1	0	1000(21)
189.5	8.9(8)	6.14(5)	189.5	0	126(5)
			123.6	65.9	80(3)
			92.4	97.1	432(10)
237.8	0.9(3)	7.11(15)	237.8	0	94(4)
			171.9	65.9	178(6)
351.9	1.1(6)	6.98(24)	351.9	0	63(6)
			286.1	65.9	35(5)
			254.8	97.1	25(1)
			162.6	189.5	128(14)
380.0	0.7(1)	7.17(7)	314.1	65.9	24(2)
			142.3	237.8	14(2)
476.1	3.8(3)	6.40(4)	476.2	0	40(2)
			379.0	97.1	291(9)
			286.4	189.5	64(8)
492.9	5.3(3)	6.25(3)	492.9	0	110(7)
			427.0	65.9	60(5)
			303.4	189.5	203(6)
			255.1	237.8	43(3)
			141.0	351.9	19(1)
514.9	8.1(6)	6.05(4)	448.9	65.9	93(9)
			417.9	97.1	314(6)
			325.4	189.5	159(4)
			162.8	351.9	103(11)
544.2	5.8(4)	6.19(4)	544.2	0	357(15)
			478.2	65.9	104(2)
			447.2	97.1	17(1)
572.1	0.6(1)	7.16(8)	334.3	237.8	30(3)
599.0	7.0(3)	6.08(3)	599.0	0	163(10)
			533.0	65.9	151(6)
			361.2	237.8	68(7)
637.9	1.9(2)	6.63(5)	572.1	65.9	84(4)
			400.0	237.8	16(3)
			286.1	351.9	35(7)
			257.9	380.0	7(2)
640.4	0.45(4)	7.30(5)	543.3	97.1	21(2)
677.0	1.7(1)	6.67(3)	611.1	65.9	63(3)
			439.3	237.8	30(2)
			297.0	380.0	5(1)
709.3	2.3(1)	6.52(3)	709.3	0	21(3)
			643.4	65.9	81(4)
			519.7	189.5	8(2)
719.2	1.5(1)	6.70(4)	719.4	0	18(3)
			653.5	65.9	24(3)
			481.2	237.8	30(3)
733.9	0.6(1)	7.09(8)	636.7	97.1	18(2)
			257.8	476.1	9(2)
770.2	0.19(2)	7.58(7)	532.3	237.8	9(1)
781.0	1.1(1)	6.81(5)	591.5	189.5	33(4)
			429.3	351.9	11(2)
			304.7	476.1	7(2)
831.5	2.7(1)	6.40(2)	831.9	0	9(2)
			734.6	97.1	39(3)

TABLE I. (Continued).

| E_i (keV)	I_β (%)	Log ft	E_γ (keV)	E_f (keV)	I_γ
			642.1	189.5	18(3)
			355.5	476.1	37(4)
			316.6	514.9	40(2)
844.7	3.0(2)	6.35(4)	655.1	189.5	58(5)
			607.0	237.8	20(3)
			492.6	351.9	12(2)
			351.8	492.9	52(5)
			206.8	637.9	12(1)
912.9	0.8(1)	6.90(6)	815.8	97.1	18(2)
			723.4	189.5	22(2)
1053.6	0.4(1)	7.14(11)	577.5	476.1	21(3)
1068.1	0.7(1)	6.89(7)	575.2	492.9	12(1)
			553.2	514.9	20(3)
1127.0	0.15(4)	7.53(12)	775.1	351.9	7(2)
1134.6	0.7(1)	6.86(7)	1037.6	97.1	10(2)
			945.0	189.5	24(4)
1147.1	0.6(1)	6.92(8)	671.1	476.1	17(2)
			632.1	514.9	10(2)
1163.6	1.0(1)	6.69(5)	1066.6	97.1	40(2)
			811.5	351.9	8(2)
1197.7	0.8(1)	6.77(6)	1008.1	189.5	10(2)
			845.8	351.9	5(1)
			721.9	476.1	6(1)
			704.7	492.9	11(1)
			682.1	514.9	6(2)
1233.0	0.47(2)	6.99(3)	688.8	544.2	22(1)
1243.8	1.1(1)	6.61(5)	728.8	514.9	21(2)
			412.4	831.5	18(2)
			399.1	844.7	12(3)
1304.2	0.25(5)	7.23(9)	789.4	514.9	10(2)
			705.1	599.0	2(1)
1351.2	0.8(1)	6.70(6)	1254.1	97.1	8(2)
			1161.2	189.5	9(2)
			836.1	514.9	10(1)
			807.0	544.2	9(2)
1368.9	0.70(5)	6.75(4)	875.8	492.9	26(2)
			770.1	599.0	7(1)
1393.1	0.6(1)	6.80(8)	917.1	476.1	4(1)
			900.6	492.9	15(3)
			877.8	514.9	10(3)
1534.8	0.7(1)	6.67(7)	1058.8	476.1	20(3)
			1019.8	514.9	12(3)
1581.4	0.6(1)	6.71(8)	1391.8	189.5	18(2)
			904.4	677.0	9(2)
1597.0	0.7(1)	6.64(7)	1121.0	476.1	15(3)
			1103.9	492.9	13(3)
			1053.1	544.2	7(2)
1632.7	1.6(1)	6.26(4)	1139.9	492.9	14(3)
			1117.8	514.9	48(4)
			994.9	637.9	15(3)
1693.7	1.3(1)	6.32(4)	1693.4	0	39(4)
			1149.5	544.2	24(5)
1740.5	0.4(1)	6.81(11)	1550.8	189.5	8(1)
			1264.4	476.1	10(3)
1952.7	1.2(1)	6.22(4)	1714.9	237.8	16(2)
			1600.8	351.9	13(3)
			1408.6	544.2	24(4)
			1275.7	677.0	4(1)
2001.1	0.5(1)	6.57(9)	1508.3	492.9	11(3)
			1456.9	544.2	14(2)
2031.4	0.23(2)	6.89(5)	1841.9	189.5	11(1)
2061.1	1.4(1)	6.09(4)	1585.8	476.1	5(2)
			1546.3	514.9	15(3)
			1516.8	544.2	47(3)
2073.8	0.5(1)	6.53(9)	1598.1	476.1	6(2)
			1558.7	514.9	16(3)
2099.2	0.4(1)	6.62(11)	1555.0	544.2	8(2)
			1500.2	599.0	12(2)
2120.4	1.2(1)	6.13(4)	2023.5	97.1	36(3)
			1605.3	514.9	20(4)
2133.7	0.6(1)	6.42(8)	2036.9	97.1	14(2)
			1657.4	476.1	6(1)
			1618.2	514.9	9(3)
2142.9	0.8(1)	6.29(6)	1953.6	189.5	8(1)
			1650.4	492.9	18(2)
			1627.7	514.9	11(3)
2161.8	0.17(2)	6.95(6)	1685.8	476.1	8(1)
2252.4	0.8(1)	6.23(6)	2186.4	65.9	18(3)
			2155.6	97.1	11(2)
			1776.2	476.1	10(2)
2311.8	0.7(1)	6.25(7)	2311.6	0	23(2)
			1835.7	476.1	8(2)
2391.6	0.38(5)	6.47(6)	1792.2	599.0	12(2)
			1715.2	677.0	6(1)
2428.2	0.19(2)	6.74(5)	1935.4	492.9	9(1)
2485.7	0.21(4)	6.69(9)	1992.8	492.9	10(2)
2570.0	2.4(2)	5.55(4)	2569.6	0	14(2)
			2504.1	65.9	23(7)
			2055.0	514.9	24(4)
			2026.3	544.2	13(2)
			1971.0	599.0	11(3)
			1931.6	637.9	27(4)
2611.2	0.34(4)	6.37(6)	2067.0	544.2	16(2)
2622.8	1.2(1)	5.82(4)	2525.7	97.1	25(3)
			2270.4	351.9	5(2)
			2147.3	476.1	13(2)
			2107.9	514.9	14(3)
2654.7	0.23(4)	6.51(8)	2557.6	97.1	11(2)
2707.9	1.1(1)	5.80(5)	2518.6	189.5	28(2)
			2214.9	492.9	10(2)
			2193.0	514.9	13(3)
2713.7	0.21(4)	6.51(9)	2237.6	476.1	10(2)
2729.8	0.38(5)	6.24(6)	2540.1	189.5	13(2)
			2186.2	544.2	5(1)
2740.7	0.40(5)	6.22(6)	2264.2	476.1	5(1)
			2197.0	544.2	14(2)
2812.0	0.6(1)	5.99(8)	2296.9	514.9	9(1)
			2268.1	544.2	8(1)
			2213.2	599.0	11(3)
2942.9	0.11(2)	6.63(9)	2466.9	476.1	5(1)
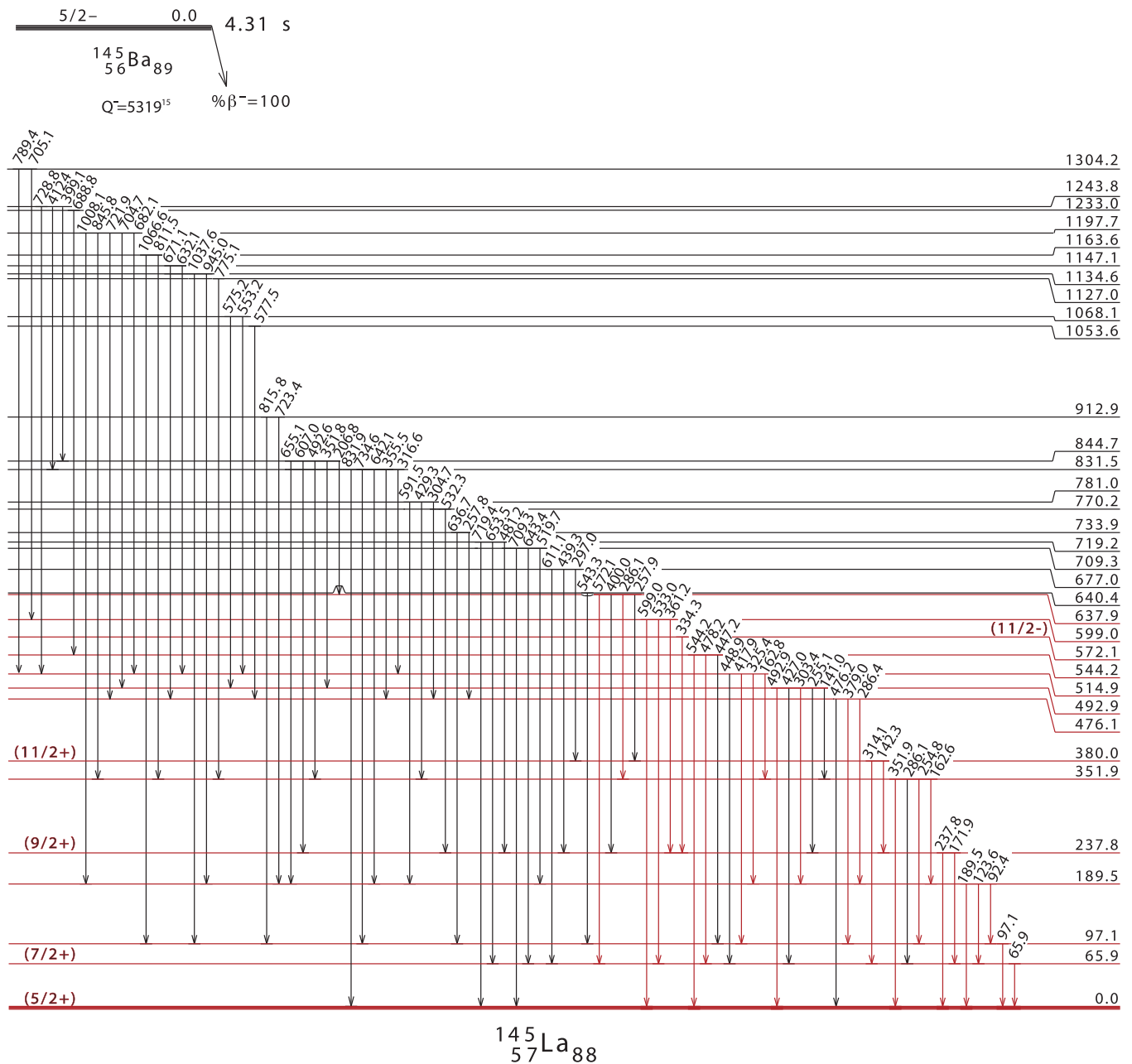
FIG. 5. Level scheme for ^{145}La (lower part). Previously reported transitions, levels, spins, and parities are drawn in red. The Q value and $T_{1/2}$ are taken from Refs. [23] and [14], respectively.

oratory website [26]. Total intensities were evaluated using measured [14] or calculated [27] internal conversion coefficients (Icc). If the multipolarity of a transition is unknown, then we took the mean value between the lower and higher Icc values calculated for E1, M1, and E2 multipolarities. Q value $= 5319(15)$ keV [23] and $T_{1/2} = 4.31(16)$ s from Ref. [14] for the ^{145}Ba $\rightarrow$ ^{145}La decay have been used in the calculations.

Figures 7, 8, and 9 show coincidence spectra, divided in different energy ranges, gated on the 65.9, 97.1, 303.4, 379.0, and 417.9 keV transitions. The first two lines correspond to the main transitions feeding the ground state. The last three lines are the strongest transitions depopulating the 492.9, 476.1, and 514.9 keV levels, respectively.

The 572.1 keV state has been reported by Urban *et al.* [4] and Zhu *et al.* [5]. In both works the spin and parity of this state have been assigned as $(11/2^-)$. Since the spin and parity of the ground state of the parent nucleus ^{145}Ba is $(5/2^-)$ a negligible β feeding is expected. In addition, we do not observe any γ-ray transition feeding the 572.1 keV state, concluding that the population of this state could be due to several non observed weak transitions or high-energy transitions.
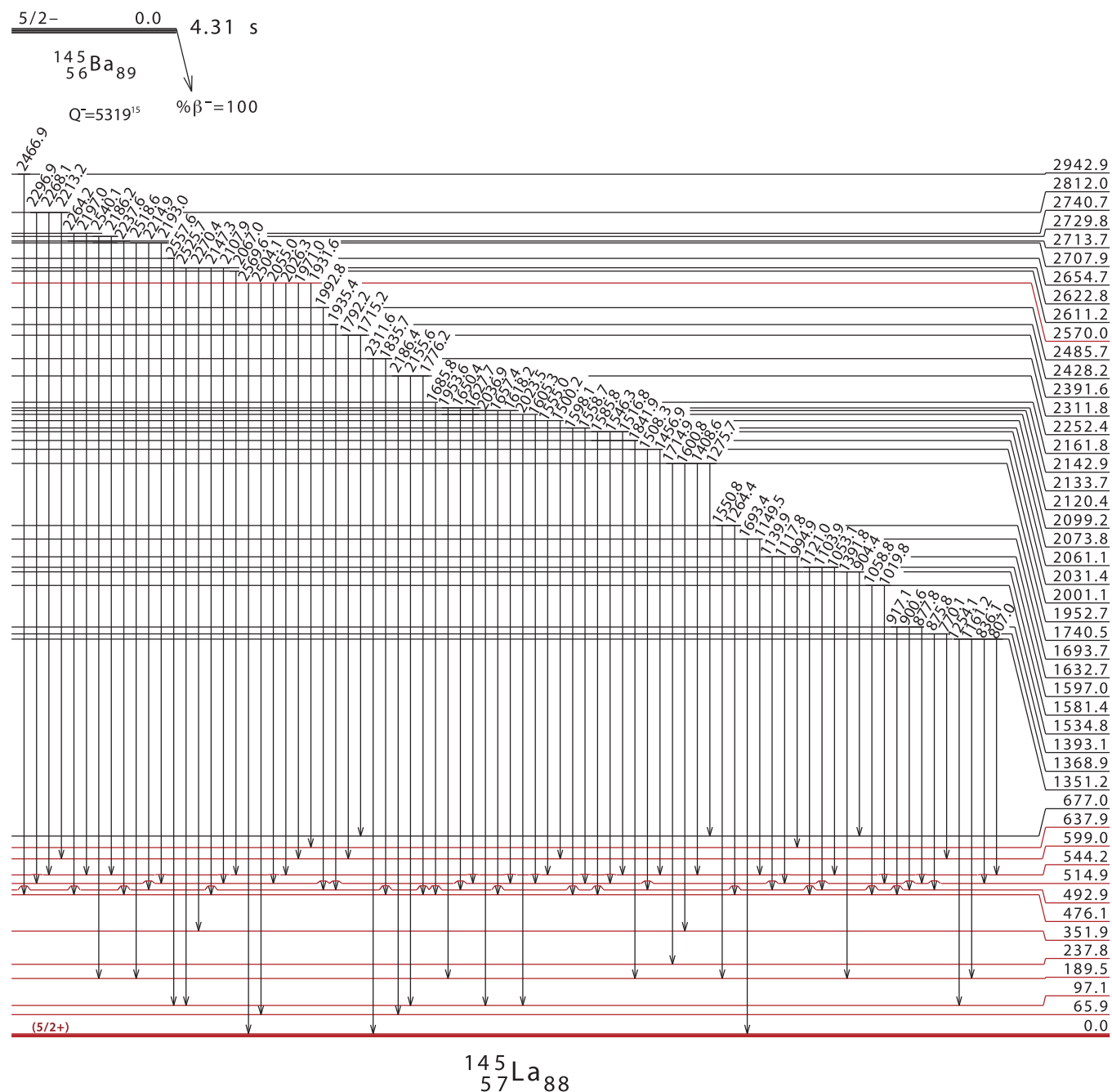
FIG. 6. Level scheme for 145La (upper part). Previously reported transitions, levels, spins, and parities are drawn in red. The Q value and $T_{1/2}$ are taken from Refs. [23] and [14], respectively.

Two pairs of transitions of similar energies are in coincidence (162.6–162.8 keV and 286.1–286.1 keV). They have been already reported and placed or placed tentatively (as in the case of the 162.8 keV line) in the level scheme [14] and we carefully tested and confirmed their presence and placement throught the analysis of the coincidence spectra. Two similar sequences (351.8–492.9 keV and 492.6–351.9 keV) link the 844.7 keV level to the ground state. The two transitions directly feeding the ground state were previously reported [14]. The other two lines (351.8 and 492.6 keV) were placed depopulating the 844.7 keV level since they were observed in coincidence with transitions de-exciting the 492.9

and 351.9 keV levels, respectively. Figures 10(a) and 10(b) show the spectra gated on the 352 and 493 keV doublets, where the lines in coincidence with each member of the doublet are indicated.

The fast-timing results were obtained from the analysis of γ-γ coincidences between the two LaBr$_3$(Ce) detectors, β-γ coincidences between the Pilot U plastic scintillator detector and the LaBr$_3$(Ce) detectors, and γ-γ-γ coincidences between the two LaBr$_3$(Ce) detectors and any Ge(HP) detector. The fast-timing method enables the determination of half-lives in the range between several tens of picoseconds to several nanoseconds and requires strong and clean γ rays. In
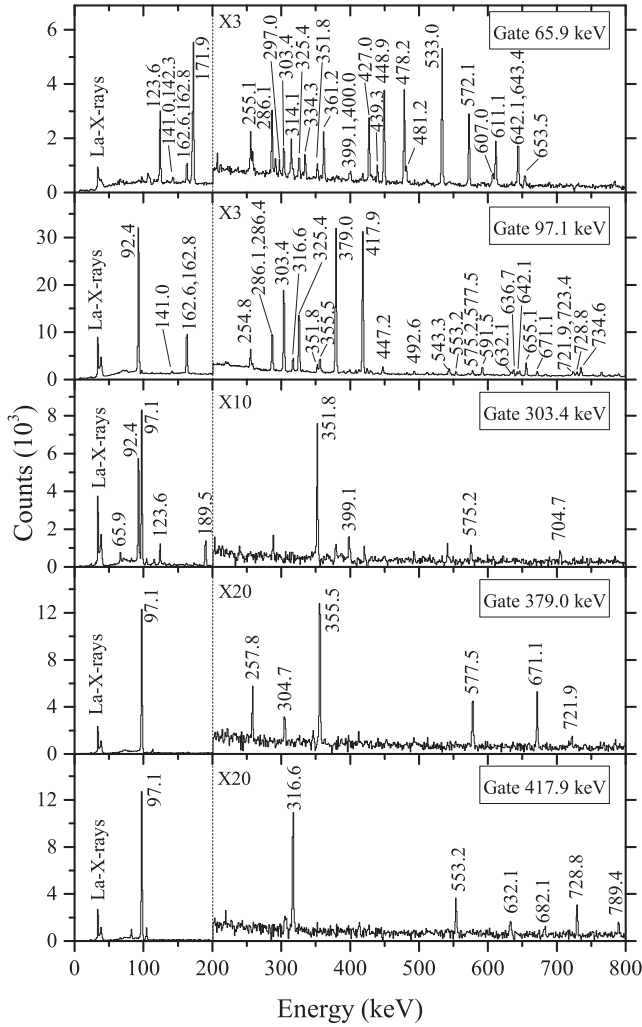
FIG. 7. Coincidence spectra in the 0–800 keV energy range. Only transitions belonging to the ^{145}Ba $\rightarrow$ ^{145}La decay are indicated.

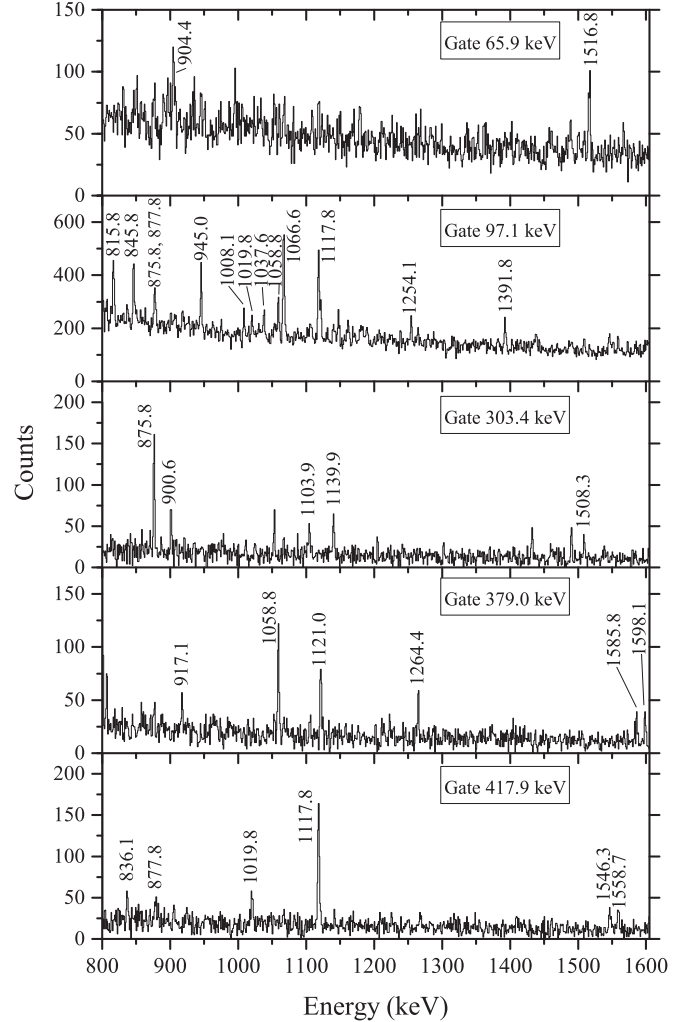FIG. 8. Coincidence spectra in the 800–1600 keV energy range. Only transitions belonging to the ^{145}Ba $\rightarrow$ ^{145}La decay are indicated.

what follows, we will use simplified labels for the detectors and TACs involved in the analysis:

A: cylindrical LaBr$_3$(Ce) detector.

B: truncated conical LaBr$_3$(Ce) detector.

β: Pilot U plastic scintillator β detector.

G: the three Ge(HP) detectors summed together.

E_i: energy corresponding to detector i.

T_{ij}: TAC corresponding to detector i as start and detector j as stop.

In Fig. 11 we illustrate the quality of the time spectra obtained with our fast-timing setup. Figures 11(a) and 11(b) show time spectra measured with a ^{60}Co calibration source, where the prompt response associated with the half-life levels of ^{60}Ni [28] was fitted with gaussian curves. FWHM time resolutions of 214 and 157 ps were obtained for the 1332.5–1173.2 keV and the β–1332.5 keV coincidences, respectively. The time-response calibration and a test of the fast-timing setup were performed using a source of ^{138}Cs which populates by β-decay excited states of ^{138}Ba of well known half-lives [29]. Figures 11(c) and 11(d) show time spectra for the half-life determination of the 1898.6 keV level

of ^{138}Ba obtained from the 462.8–547.0 keV and β–462.8 keV coincidences, respectively. In Fig. 11(d) the slope is assigned to the half-life of the level of interest since contributions of levels above the 1898.6 keV can be considered negligible as discussed in Ref. [13]. The fit of the spectra in Figs. 11(c) and 11(d) with an exponential decay gave values of the half-life of the 1898.6 keV level of $T_{1/2} = 2.11(5)$ ns and $T_{1/2} = 2.14(3)$ ns, respectively, in good agreement with the adopted value of 2.160(11) ns [29]. Figures 11(a) and 11(c) were obtained from the $E_A E_B T_{AB}$ cube and Figs. 11(b) and 11(d) from the $E_A E_\beta T_{\beta A}$ cube. The analysis of the shape of prompt time spectra, in particular of their slight deviations from a true Gaussian [13,20] allowed us to determine the $T_{1/2}$ lower limit that can be measured using the deconvolution method: $\sim$50 ps from β-LaBr$_3$(Ce) measurements and $\sim$100 ps from LaBr$_3$(Ce)-LaBr$_3$(Ce) (*A-B*) measurements.

The examination of time spectra corresponding to levels of ^{145}La revealed that the levels at 65.9 and 97.1 keV have half-lives in the nanosecond range.

In Fig. 12 we show several time spectra used in the determination of the half-life of the 65.9 keV level. Figure 12(a)
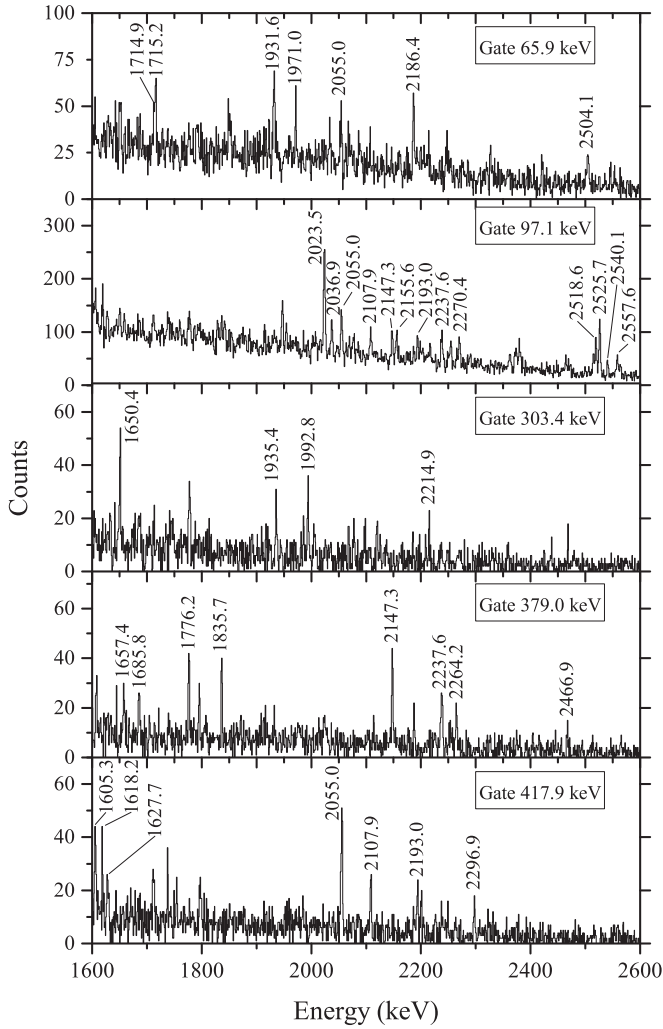
FIG. 9. Coincidence spectra in the 1600–2600 keV energy range. Only transitions belonging to the ^{145}Ba $\rightarrow$ ^{145}La decay are indicated.
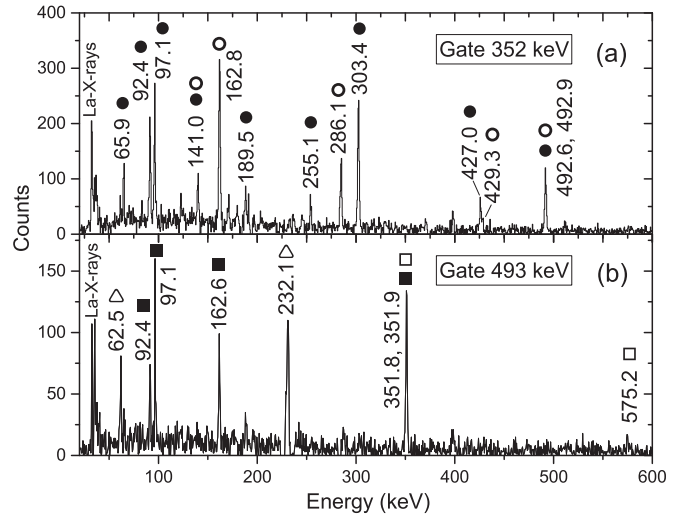

FIG. 10. Coincidence spectra gated on the (a) 352 keV and (b) 493 keV doublets. In panel (a) peaks in coincidence with the 351.8 (351.9) keV line are indicated by a full (open) circle. In panel (b) peaks in coincidence with the 492.6 (492.9) keV line are indicated by a full (open) square. Peaks marked with open triangles are in coincidence with the 492.2 keV line corresponding to the ^{145}Ce $\rightarrow$ ^{145}Pr decay.

shows the relevant portion of the two-dimensional energy projection of the $E_A E_B T_{AB}$ cube, where two gated regions associated with the 171.9–65.9 keV start-stop coincidences and the reversed 65.9–171.9 keV combination are indicated in red and blue, respectively (full line-dot for peaks and dash line-dot for backgrounds). The two background-subtracted time spectra obtained by gating on both regions are displayed in Fig. 12(b) with the corresponding colors. The fit of the slopes using an exponential decay gave the values of $T_{1/2} = 1.83(9)$ ns and $T_{1/2} = 1.89(8)$ ns. Figure 12(c) displays the T_{AB} spectrum gated on the 65.9 keV line in A, any energy in B, and an additional gate on the 123.6 or 171.9 keV lines on G. This time spectrum does not involve any contamination from ^{145}Ce and, even if the statistics in (c) is poorer than in (b) and we neglected the energy dependence time response in B, we obtained a similar value for the half-life. This enable us to consider the contamination from the 64.3–169.8 keV coincidence in ^{145}Ce with $T_{1/2} = 13(3)$ ns [14] as nonsignificant. The time spectrum in Fig. 12(d) was obtained from the $E_A E_\beta T_{\beta A}$ cube. Even if the time spectrum involves all the contributions of the states belonging to the decay path

to the 65.9 keV level, we obtained again a similar half-life value. The extracted values were weighted by its squared errors, obtaining $T_{1/2} = 1.80(4)$ ns for the 65.9 keV level. This value differs strongly from the $T_{1/2} = 9(2)$ ns reported by the evaluators [14]. But it could be in agreement with the results of the original publication [30] where Clark *et al.* referred to a $T_{1/2} < 8$ ns value associated with a 66.0(1) keV transition assigned to ^{146}La but with an uncertainty of 1 unit in the mass determination.

The half-life of the level located at 97.1 keV was extracted from the analysis of several time spectra. Figure 13 displays two time spectra and the corresponding gated regions (peaks and backgrounds) in the two-dimensional energy projection of the $E_A E_B T_{AB}$ cube. Since the energy resolution of the
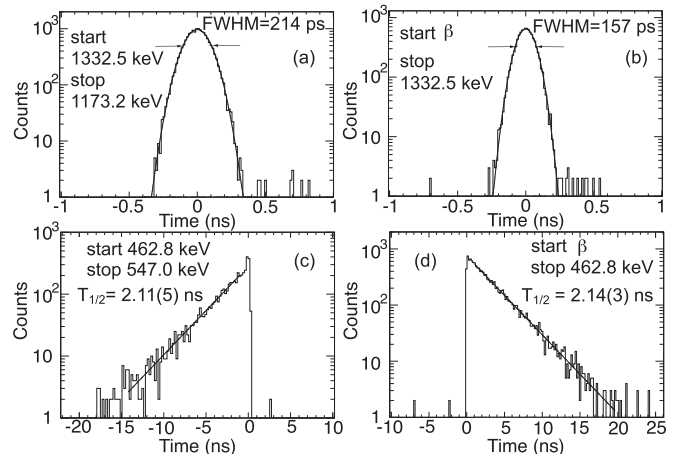

FIG. 11. Time spectra obtained with a ^{60}Co calibration source (upper part) and the 1898.6 keV level of ^{138}Ba (lower part).
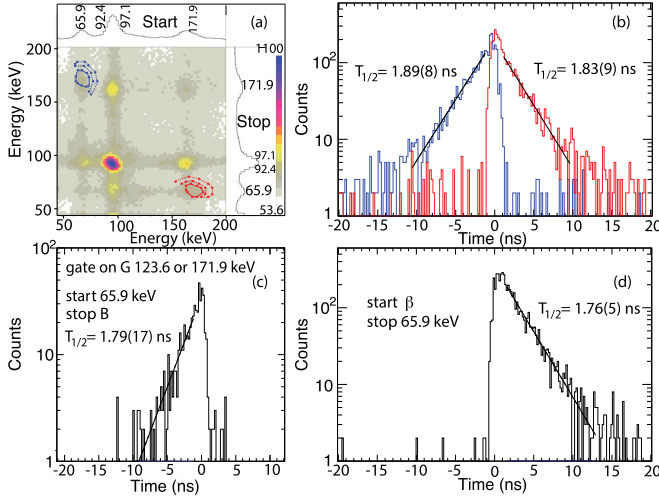
FIG. 12. Spectra corresponding to the determination of the half-life of the 65.9 keV level: (a) Two-dimensional energy projection of the $E_A E_B T_{AB}$ cube, (b) time spectra obtained by gating on the regions indicated in panel (a), (c) time spectra with the G gating conditions, and (d) time spectra from β-γ coincidences.

LaBr$_3$(Ce) detectors is not good enough to discriminate between the 92.4 and the 97.1 keV lines, the gate showed in Fig. 13(a) corresponds to both, the 92.4–97.1 keV start-stop coincidence and the 97.1–92.4 keV reversed combination and, hence, the time spectrum in Fig. 13(b) displays two similar slopes on both sides. The fit of the slopes gave the values of $T_{1/2} = 1.99(3)$ ns and $T_{1/2} = 1.97(3)$ ns. In Fig. 13(c) two peaks are indicated representing the 379.0–97.1 keV and 417.9–97.1 keV coincidences. The time spectra gated on these two peaks were added to increase statistics, and the
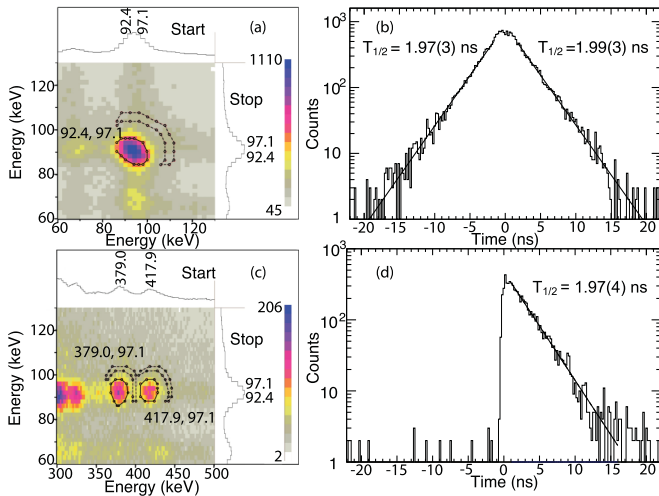

FIG. 13. Spectra corresponding to the determination of the half-life of the 97.1 keV level: (a) Two-dimensional energy projection of the $E_A E_B T_{AB}$ cube showing the 92.4–97.1 keV coincidence, (b) time spectra obtained setting the gate marked in panel (a), (c) two-dimensional energy projection of the $E_A E_B T_{AB}$ cube showing the 379.0–97.1 keV and the 417.9–97.1 keV coincidences, and (d) sum of time spectra obtained setting the gates indicated in panel (c).
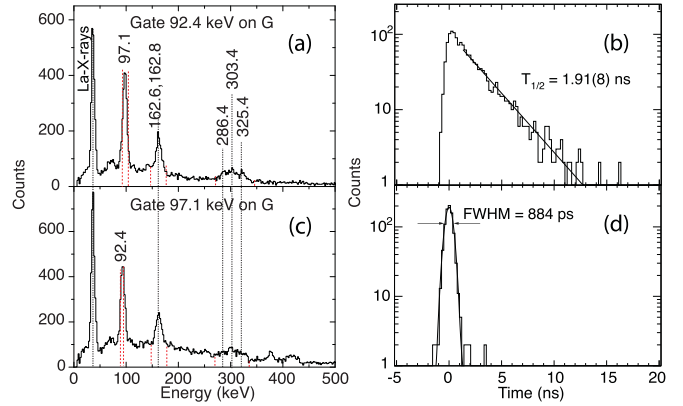

FIG. 14. (a) E_A projection of the $E_A E_B T_{AB}$ cube gated on the 92.4 keV line in the Ge(HP) detectors. (b) Time spectrum corresponding to the 97.1 keV level obtained from the G 92.4 keV-gated $E_A E_B T_{AB}$ cube. See text for the contribution of the 189.5 keV level. (c) Same as (a) but with a gate on the 97.1 keV line. (d) Time spectrum corresponding to the 189.5 keV level obtained from the G 97.1 keV-gated $E_A E_B T_{AB}$ cube.

obtained spectrum is displayed in Fig. 13(d), which was then fitted by an exponential decay curve resulting in the value of $T_{1/2} = 1.97(4)$ ns. Figure 14(a) shows the E_A projection of the $E_A E_B T_{AB}$ cube constructed demanding a gate on the 92.4 keV line in the Ge(HP) detectors to exclude this transition in the LaBr$_3$(Ce) detectors and isolate the 97.1 keV line. The three regions used as energy gates are indicated, delimited by red dashed lines. The same regions were defined on the E_B axis. Figure 14(b) is the sum of four time spectra, two gated on the 162.6–162.8 keV (start A)–97.1 keV (stop B) and on the 286.4–303.4–325.4 keV (start A)–97.1 keV (stop B) coincidences, and two from the reversed combinations. The antidelayed spectra were flipped around time zero before being added. The fit of the slope corresponds to an exponential decay with $T_{1/2} = 1.91(8)$ ns. This value involves the half-lives of the 189.5 and 97.1 keV levels. Figure 15(a) shows the time distribution and the exponential decay fit of the coincidence between the β particles (start β) and the 92.4 and 97.1 keV γ rays (stop A). The prompt contribution due to the 92.4 keV line (see below) has been reduced setting the gate on A in the right part of the peak. The half-life extracted, $T_{1/2} = 2.00(3)$ ns, contains not only the contribution of the 97.1 keV level but also of the levels of higher energy fed by β radiations and decaying to the 97.1 keV level. However, it is in agreement with the values obtained in the analysis of Figs. 13(b), 13(d), and 14(b) suggesting that contributions to the slope from levels above 97.1 keV can be neglected. In particular it will be demonstrated later in this section that it is the case for the levels located at 189.5, 476.1, and 514.9 keV. The weighted average of the different values obtained for the 97.1 keV level is $T_{1/2} = 1.98(2)$ ns.

To analyze the half-life of the 189.5 keV level an $E_A E_B T_{AB}$ cube was constructed demanding a gate on the 97.1 keV line in the Ge(HP) detectors to exclude this transition in the LaBr$_3$(Ce) detectors and isolate the 92.4 keV line, the strongest line which depopulates the level of interest. The
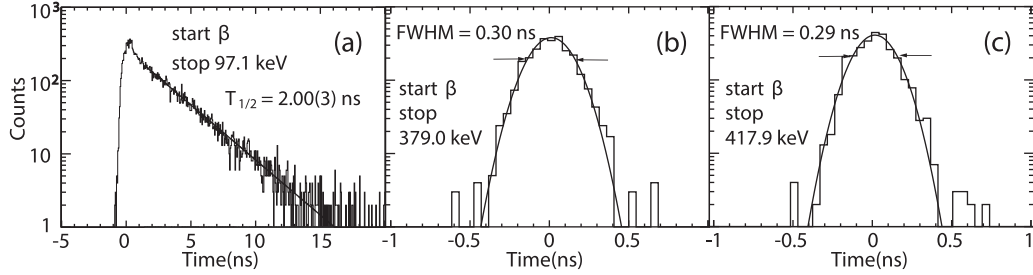
FIG. 15. Time spectra corresponding to: (a) 97.1 keV level, (b) 476.1 keV, and (c) 514.9 keV, obtained setting gates on β (start) and A (stop).

analysis was performed in a similar way of that mentioned before for the 97.1 keV level. Figure 14(c) shows the E_A projection of this cube and Fig. 14(d) corresponds to the sum, previously matched, of the four obtained time spectra. The shape of the four spectra suggests prompt coincidences. The resulting time distribution was fitted by a Gaussian curve resulting in a FWHM of 884 ps, consistent with the expected time resolution at these energies. This analysis shows that the 189.5 keV level has a half-life shorter than the limit that can be reached by the deconvolution method: $T_{1/2}$(189.5 keV level) $\lesssim$ 100 ps. Because of the low-energy of the transition involved, it was not possible to give a more precise $T_{1/2}$ value by applying the centroid shift method.

Figures 15(b) and 15(c) show the time distributions corresponding to the 379.0 and 417.9 keV γ rays detected in A in coincidence with the β particles. Both curves display symmetric gaussian shapes with FWHM values around 300 ps as expected for the time resolution of $T_{\beta A}$ at these energies. The centroid shift method was applied to these spectra for evaluating the half-lives of the 476.1 and 514.9 keV levels. It is worth mentioning that the values obtained for these levels include the half-lives of all the levels that feed them. We first obtained the prompt centroid position as a function of the γ-ray energy by using known states with half-lives shorter than 10 ps belonging to ^{138}Ba directly populated by β-decay from ^{138}Cs [29]. Figure 16 shows the prompt response of $T_{\beta A}$, the centroid of the time response for the 409, 547, 1010 keV lines of ^{138}Ba after correction from their half-lives are plotted with open circles and the prompt curve through the data points is drawn. The difference between the centroids corresponding to the 379.0 and 417.9 keV peaks and the prompt curve established upper limits of 18 and 20 ps to the half-lives of the 476.1 and 514.9 keV levels, respectively.

Table II shows the half-life values obtained in the present work together with previously reported values. The values presented in Table II are the only ones that could be determined.

IV. DISCUSSION

Assuming $\epsilon_2 = 0.16$ and $\epsilon_4 = -0.05$ [31] for the nuclear deformation of the ground state of ^{145}La, five Nilsson orbitals lie near the Fermi level: $g_{7/2}$ (5/2$^+$[413]) and $d_{5/2}$ (3/2$^+$[411]), corresponding to a pseudospin doublet, and $h_{11/2}$ (1/2$^-$[550],

3/2$^-$[541], 5/2$^-$[532]). In Refs. [4,5] the ground state and the levels at 65.9, 237.8, and 380.0 keV have been proposed to belong to the ground-state band built on the $g_{7/2}$ proton orbital, with $I^\pi = 5/2^+$, $7/2^+$, $9/2^+$, and $11/2^+$, respectively. These assignments are corroborated by the good agreement between the experimental and theoretical $(1 + \delta^2)B(M1)/B(E2)$ ratios presented in Table III. The experimental ratios, in units of $\mu_N^2/(eb)^2$, were determined by the following expression [32]:

$$(1 + \delta^2)\frac{B(M1, I \to I - 1)}{B(E2, I \to I - 2)} = 0.697\frac{E_{\gamma_2}^5}{E_{\gamma_1}^3}\frac{1}{\lambda},$$

where E_{γ_1, γ_2} are the energies (in MeV) corresponding to the $\Delta I = 1, 2$ transitions, respectively, δ is the E2/M1 multipole mixing ratio, and λ the γ-ray intensity ratio $I(\gamma_2)/I(\gamma_1)$.

For the theoretical estimates of the reduced transition probabilities we used the expressions for a rotational band with good quantum number K, assuming axial symmetry,
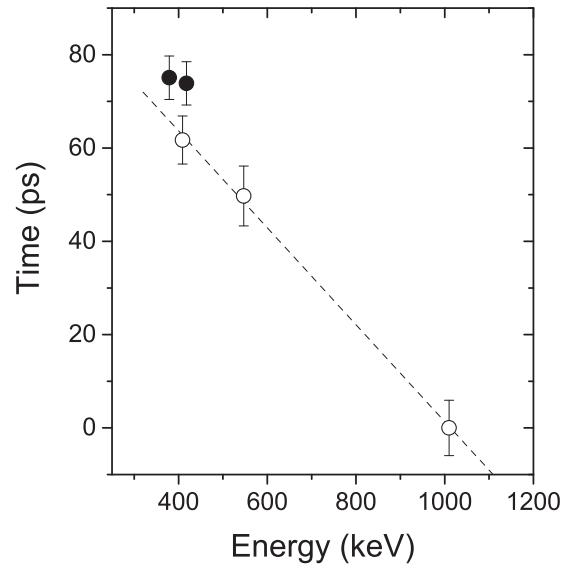

FIG. 16. Prompt centroid of $T_{\beta A}$ as a function of γ-ray energy measured in A obtained from the 409, 547, and 1010 keV lines of ^{138}Ba (open circles) and the linear fit through these data points (dashed line). The centroids corresponding to the 379.0 and 417.9 keV lines of ^{145}La are plotted with full circles.

TABLE II. Half-life values obtained in the present work and previously reported values.

E_{level} (keV)	$T_{1/2}$ (present work)	$T_{1/2}$ (reported values)
65.9	1.80(4) ns	9(2) ns [14], < 8 ns [30]
97.1	1.98(2) ns	
189.5	$\lesssim 100$ ps	
476.1	<18 ps	
514.9	<20 ps	

$K = \Omega \neq \frac{1}{2}$ [33]:

$$B(M1, I \rightarrow I-1) = \frac{3}{4\pi}(g_K - g_R)^2 K^2 \langle IK10|(I-1)K \rangle^2,$$

$$B(E2, I \rightarrow I-2) = \frac{5}{16\pi}Q_0^2 \langle IK20|(I-2)K \rangle^2,$$

$$\delta^2 = 0.286 E_\gamma^2 \frac{Q_0^2}{(g_K - g_R)^2 K^2} \frac{\langle IK20|(I-1)K \rangle^2}{\langle IK10|(I-1)K \rangle^2},$$

where g_K and $g_R = Z/A$ are the proton and the collective gyromagnetic factors, respectively. The proton g factors were calculated by the expression [33]

$$g_K = g_l + (g_s - g_l)\frac{\langle s_3 \rangle}{K}.$$

The expectation values of the spin projection on the symmetry axis, $\langle s_3 \rangle$, were evaluated using Nilsson type wave functions obtained from the diagonalization of the deformed harmonic oscillator with the ϵ_2 and ϵ_4 values mentioned above and parameters κ and μ extracted from Ref. [34]. For the proton orbital and spin g-factors we used: $g_l = 1$ and $g_s = 3.91$. Q_0 is the intrinsic quadrupole moment given by

$$Q_0 = \frac{3ZeR_0^2}{\sqrt{5\pi}}\beta\left(1 + \frac{2}{7}\sqrt{\frac{5}{\pi}}\beta\right),$$

with $\epsilon_2 \approx 0.95\beta$, and neglecting the hexadecapole contribution.

In addition, the theoretical $B[M1, 7/2^+(5/2^+[413]) \rightarrow 5/2^+(5/2^+[413])] = 0.0156 \mu_N^2$ is in very good agreement with the experimental value [0.0165(7) μ_N^2] obtained from the half-life measured in this work for the 65.9 keV level assuming a pure M1 65.9 keV transition [14]. This excellent agreement supports the configuration assignments.

TABLE III. Experimental and theoretical $(1+\delta^2)B(M1, I \rightarrow I-1)/B(E2, I \rightarrow I-2)$ ratios.

Orbital	I ($\hbar$)	Experimental (μ_N^2/e^2b^2)	Theoretical (μ_N^2/e^2b^2)
$5/2^+$ [413]	9/2	0.20(2)	0.30
	11/2	0.43(10)	0.19
$3/2^+$ [411]	7/2	0.89(13)	2.4
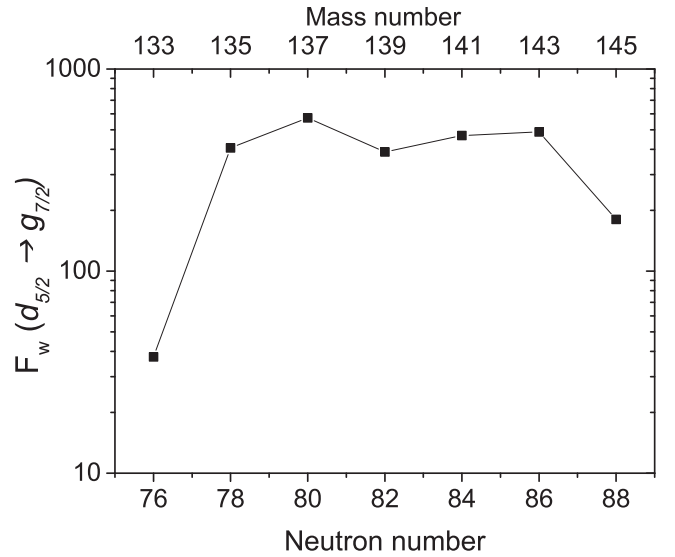
FIG. 17. Hindrance factors with respect to the Weisskopf estimate for the $d_{5/2} \rightarrow g_{7/2}$ transition in odd $^{133-145}$La nuclei. The $F_w(^{133}$La) value corresponds to the upper limit.

The parity of the levels at 97.1, 189.5, and 351.9 keV have been suggested as being positive [14] and their decay patterns are compatible with $I^\pi = 3/2^+$, $5/2^+$, and $7/2^+$, respectively. In ^{133}La, the $d_{5/2}$ ($3/2^+[411]$) proton orbital is the main contribution to the $3/2^+$ 97.259 keV level and the configuration of the ground state is a mixture between the $g_{7/2}$ ($5/2^+[413]$) and $d_{5/2}$ ($5/2^+[402]$) orbitals [35]. In ^{145}La, symmetric to ^{133}La with respect to $N = 82$, the situation of the 97.1 keV level seems to be similar excepting the half-life (<0.4 ns in ^{133}La [35] and 1.98(2) ns in ^{145}La). In Fig. 17 we plot the hindrance factors with respect to the Weisskopf estimate (F_w) for the M1 transitions between the lower levels suggested to correspond to the $d_{5/2}$ and $g_{7/2}$ configurations (l-forbidden M1 transitions) for the odd $^{133-145}$La nuclei. Data for $^{133-143}$La correspond to Refs. [35–40]. In ^{133,145}La the transition corresponds to $3/2^+ \rightarrow 5/2^+$, in $^{137-143}$La to $5/2^+ \rightarrow 7/2^+$, and in ^{135}La, where the transition corresponds to $7/2^+$ ($g_{7/2}$) $\rightarrow 5/2^+$ ($d_{5/2}$), the F_w has been modified by the $\frac{6}{8}$ factor corresponding to $(2I_f + 1)/(2I_i + 1)$. These values fall within the F_w range observed for all the $d_{5/2} \rightarrow g_{7/2}$ transitions known in the $51 \leqslant Z \leqslant 63$ nuclei [13]. In the lanthanum isotopes, the F_w values are very similar for neutron number around $N = 82$ and decrease for further ones ($N = 76$ and 86), indicating that the configurations involved in the description of the states are less pure as the neutron number differs from $N = 82$. Therefore, the smaller value observed for ^{133}La than for ^{145}La could be due to a greater mixing of the $g_{7/2}$ and $d_{5/2}$ orbitals in the configuration of the ground state in ^{133}La than in ^{145}La. We propose that the levels at 97.1, 189.5, and 351.9 keV are members of the band built mainly on the $d_{5/2}$ ($3/2^+[411]$) proton orbital. These assignments are also supported by the small difference in the excitation energy expected between the two partners of the pseudospin doublet $g_{7/2}$ ($5/2^+[413]$)–$d_{5/2}$ ($3/2^+[411]$) and the agreement between the experimental and theoretical $(1 + \delta^2)B(M1)/B(E2)$ ratios (see Table III).
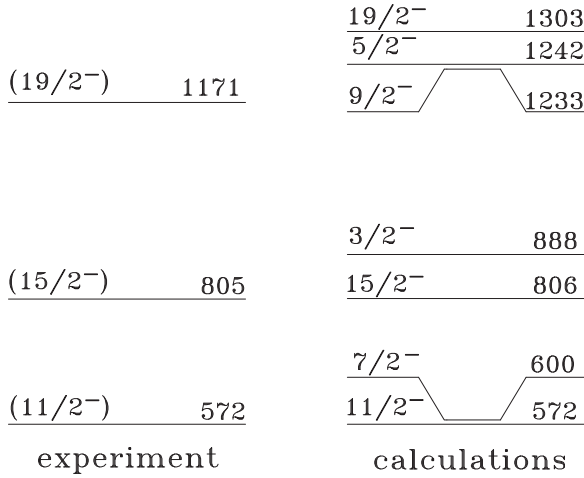
FIG. 18. Experimental and calculated negative parity levels.

As mentioned before, the $11/2^-$ state at 572.1 keV has been reported as the lower observed state belonging to a decoupled rotational band based on a $h_{11/2}$ excitation [4,5]. In Fig. 18 we plotted the first experimental levels of the band together with the levels calculated in the framework of the rigid-triaxial-rotor-plus-quasiparticle model [41]. In the calculations we used an inertia parameter $\hbar^2/2\mathfrak{I} = 33.2$ keV extracted from the energy of the first 2^+ state in ^{144}Ba. The Nilsson single particle states were obtained through the diagonalization of the deformed harmonic oscillator within the $N = 5$ oscillator shell, using $\epsilon_2 = 0.16$, $\epsilon_4 = -0.05$, and the parameters κ and μ extracted from [34]. The Fermi level was set 137 keV below the $1/2^-$[550] orbital, and the pairing gap $\Delta = 0.866$ MeV was extracted from the odd-even mass difference. The energy of the calculated $11/2^-$ state was fixed to match the experimental value. The calculations predict a $7/2^-$ state very close above the $11/2^-$. In fact, the $7/2^-$ state has been observed close to the $11/2^-$ in ^{147}La and ^{149}La [42,43]. In this context a possible candidate for the $7/2^-$ state is the 599.0 keV level. This assignment is consistent with the decay pattern of the level and the log $ft = 6.08(3)$ value that suggests an allowed β transition.

The log ft values corresponding to the levels located at 476.1, 492.9, 514.9, and 544.2 keV suggest that they could have negative parity. Nevertheless, these levels with $I^\pi \leqslant 7/2^-$ could not be interpreted in the framework of the rigid-triaxial-rotor-plus-quasiparticle model. They could correspond to particle states coupled to the low-lying negative-parity states of the even-even core [44].

The log ft values for the 2570.0, 2622.8, 2707.9, and 2812.0 keV levels strongly suggest allowed β transitions and hence, negative parity. Since their decay patterns only restrict the spins for the two first levels, we propose for these four levels $I^\pi = (5/2^-, 7/2^-)$, $(5/2^-)$, $(3/2^-, 5/2^-, 7/2^-)$, and $(3/2^-, 5/2^-, 7/2^-)$, respectively.

V. CONCLUSIONS

The low-spin states in the neutron-rich ^{145}La nucleus have been studied through the beta-decay of ^{145}Ba. ^{145}Ba and its parent ^{145}Cs were produced by the photofission of ^{238}U induced by a 50 MeV electron beam impinging a UC$_x$ target at the ALTO facility. The ^{145}La low-spin state level scheme has been established from γ-γ coincidence measurements and considerably extended: 53 new levels, involving 122 transitions in their de-excitation modes. This new level scheme could be used for a more precise determination of the β^--branching intensities through the TAGS measurements. This work reports on the first results obtained with the BEDO decay station in fast-timing mode. The half-lives of the levels located at 65.9 and 97.1 keV have been measured: $T_{1/2} = 1.80(4)$ and 1.98(2) ns, respectively. The 1.80(4) ns result obtained for the 65.9 keV level refutes the value retained by the evaluators, probably erroneously, since the original article only mentioned an upper limit. For three other levels located at 189.5, 476.1 and 514.9 keV, $T_{1/2}$ upper limits have been determined: 100, 18, and 20 ps, respectively. The analysis of the properties of the first excited states, namely, the decay modes, the log ft values, the reduced transition probabilities, the Weisskopf hindrance factors, allowed us to identify the first members of the bands corresponding to the $g_{7/2}$, $d_{5/2}$, and $h_{11/2}$ proton configurations. The systematics through the La isotopes from $N = 76$ (^{133}La) to 88 (^{145}La) indicates that the mixing of the $g_{7/2}$ and $d_{5/2}$ orbitals in the configuration describing the ground state is smaller in ^{145}La than in ^{133}La.

[1] W. Nazarewicz, P. Olanders, I. Ragnarsson, J. Dudek, G. Leander, P. Möller, and E. Ruchowsa, Nucl. Phys. A **429**, 269 (1984).

[2] W. R. Phillips, I. Ahmad, H. Emling, R. Holzmann, R. V. F. Janssens, T. L. Khoo, and M. W. Drigert, Phys. Rev. Lett. **57**, 3257 (1986).

[3] B. Pritychenko, M. Birch, B. Singh, and M. Horoi, At. Data Nucl. Data Tables **107**, 1 (2016).

[4] W. Urban, W. R. Phillips, J. L. Durell, M. A. Jones, M. Leddy, C. J. Pearson, A. G. Smith, B. J. Varley, I. Ahmad, L. R. Morss, M. Bentaleb, E. Lubkiewicz, and N. Schulz, Phys. Rev. C **54**, 945 (1996).

[5] S. J. Zhu, J. H. Hamilton, A. V. Ramayya, M. G. Wang, J. K. Hwang, E. F. Jones, L. K. Peker, B. R. S. Babu, G. Drafta, W. C. Ma, G. L. Long, L. Y. Zhu, M. Li, C. Y. Gan, T. N. Ginter, J. Kormicki, J. K. Deng, D. T. Shi, W. E. Collins, J. D. Cole, R. Aryaneinejad, M. W. Drigert, J. O. Rasmussen, R. Donangelo, J. Gilat, S. Asztalos, I. Y. Lee, A. O. Macchiavelli, S. Y. Chu, K. E. Gregorich, M. F. Mohar, M. A. Stoyer, R. W. Lougheed, K. J. Moody, J. F. Wild, S. G. Prussin, G. M. Ter-Akopian, A. V. Daniel, and Y. T. Oganessian, Phys. Rev. C **59**, 1316 (1999).

[6] R. F. Casten, D. D. Warner, D. S. Brenner, and R. L. Gill, Phys. Rev. Lett. **47**, 1433 (1981).

[7] T. Yoshida and A. L. Nichols, Assessment of Fission Product Decay Data for Decay Heat Calculations, Tech. Rep. V.25 (Nuclear Energy Agency, 2007).

[8] J. Hamilton, Y. Luo, J. Hwang, E. Jones, A. Ramayya, S. Zhu, P. Gore, C. Beyer, J. Kormicki, X. Zhang, T. Ginter, M. Wang, J. Cole, M. Drigert, W. Ma, P. Varmette, G. Ter-Akopian, Y. Oganessian, A. Daniel, J. Kliman, J. Rasmussen, I. Lee, R. Donangelo, and A. de Lima, Acta Phys. Pol. B **32**, 957 (2001).

[9] S. J. Zhu, M. Sakhaee, J. H. Hamilton, A. V. Ramayya, N. T. Brewer, J. K. Hwang, S. H. Liu, E. Y. Yeoh, Z. G. Xiao, Q. Xu, Z. Zhang, Y. X. Luo, J. O. Rasmussen, I. Y. Lee, K. Li, and W. C. Ma, Phys. Rev. C **85**, 014330 (2012).

[10] G. S. Simpson, W. Urban, J. Genevey, R. Orlandi, J. A. Pinston, A. Scherillo, A. G. Smith, J. F. Smith, I. Ahmad, and J. P. Greene, Phys. Rev. C **80**, 024304 (2009).

[11] Y. Kojima, A. Taniguchi, M. Shibata, E. Oyama, T. Nishimura, K. Shizuma, and Y. Kawase, Eur. Phys. J. A **19**, 77 (2004).

[12] R. Licǎ, G. Benzoni, T. R. Rodríwguez, M. J. G. Borge, L. M. Fraile, H. Mach, A. I. Morales, M. Madurga, C. O. Sotty, V. Vedia, H. De Witte, J. Benito, R. N. Bernard, T. Berry, A. Bracco, F. Camera, S. Ceruti, V. Charviakova, N. Cieplicka-Oryńczak, C. Costache, F. C. L. Crespi, J. Creswell, G. Fernandez-Martínez, H. Fynbo, P. T. Greenlees, I. Homm, M. Huyse, J. Jolie, V. Karayonchev, U. Köster, J. Konki, T. Kröll, J. Kurcewicz, T. Kurtukian-Nieto, I. Lazarus, M. V. Lund, N. Mărginean, R. Mărginean, C. Mihai, R. E. Mihai, A. Negret, A. Orduz, Z. Patyk, S. Pascu, V. Pucknell, P. Rahkila, E. Rapisarda, J. M. Regis, L. M. Robledo, F. Rotaru, N. Saed-Samii, V. Sánchez-Tembleque, M. Stanoiu, O. Tengblad, M. Thuerauf, A. Turturica, P. Van Duppen, and N. Warr (IDS Collaboration), Phys. Rev. C **97**, 024305 (2018).

[13] B. Roussière, M. A. Cardona, I. Deloncle, D. Hojman, J. Kiener, P. Petkov, D. Tonev, Ts. Venkova, and ALTO Collaboration, Eur. Phys. J. A **47**, 106 (2011).

[14] E. Browne and J. Tuli, Nucl. Data Sheets **110**, 507 (2009).

[15] R. Greenwood, R. Helmer, M. Putnam, and K. Watts, Nucl. Instrum. Methods Phys. Res., Sect. A **390**, 95 (1997).

[16] Y. Shima, Y. Kojima, H. Hayashi, A. Taniguchi, and M. Shibata, Nucl. Data Sheets **120**, 30 (2014).

[17] S. Essabaa, N. Barré-Boscher, M. C. Mhamed, E. Cottereau, S. Franchoo, F. Ibrahim, C. Lau, B. Roussière, A. Saïd, S. Tusseau-Nenez, and D. Verney, Nucl. Instrum. Methods Phys. Res., Sect. B **317, Part B**, 218 (2013).

[18] S. Sundell and H. Ravn, Nucl. Instrum. Methods Phys. Res., Sect. B **70**, 160 (1992).

[19] A. Etilé, D. Verney, N. N. Arsenyev, J. Bettane, I. N. Borzov, M. Cheikh Mhamed, P. V. Cuong, C. Delafosse, F. Didierjean, C. Gaulard, N. Van Giai, A. Goasduff, F. Ibrahim, K. Kolos, C. Lau, M. Niikura, S. Roccia, A. P. Severyukhin, D. Testov, S. Tusseau-Nenez, and V. V. Voronov, Phys. Rev. C **91**, 064317 (2015).

[20] H. Mach, R. Gill, and M. Moszyński, Nucl. Instrum. Methods Phys. Res., Sect. A **280**, 49 (1989).

[21] J. Le Bris *et al.*, Tech. Rep. Internal Report IPNO 0603 (English version), Rapport Interne IPNO 0504 (French version).

[22] A. Sonzogni, Nucl. Data Sheets **93**, 599 (2001).

[23] M. Wang, G. Audi, F. Kondev, W. Huang, S. Naimi, and X. Xu, Chin. Phys. C **41**, 030003 (2017).

[24] "Ensdat code," http://www.nndc.bnl.gov.

[25] B. Pfeiffer, F. Schussler, J. Blachot, S. Feenstra, J. van Klinken, H. Lawin, E. Monnand, G. Sadler, H. Wollnik, and K. Wünsch, Z. Phys. A: At. Nucl. **287**, 191 (1978).

[26] "Logft code," http://www.nndc.bnl.gov.

[27] T. Kibédi, T. Burrows, M. Trzhaskovskaya, P. Davidson, and C. Nestor, Nucl. Instrum. Methods Phys. Res., Sect. A **589**, 202 (2008).

[28] E. Browne and J. Tuli, Nucl. Data Sheets **114**, 1849 (2013).

[29] J. Chen, Nucl. Data Sheets **146**, 1 (2017).

[30] R. G. Clark, L. E. Glandenin, and W. L. Talbert, Jr., Proc. Symp. Phys. Chem. Fission **II**, 221 (1973).

[31] P. Möller, A. Sierk, T. Ichikawa, and H. Sagawa, At. Data Nucl. Data Tables **109-110**, 1 (2016).

[32] K. E. G. Löbner, *The Electromagnetic Interaction in Nuclear Spectroscopy*, edited by W. D. Hamilton (North-Holland, Amsterdam, 1975).

[33] A. Bohr and B. Mottelson, *Nuclear Structure*, Vol. II (World Scientific, Singapore, 1998).

[34] T. Bengtsson and I. Ragnarsson, Nucl. Phys. A **436**, 14 (1985).

[35] Y. Khazov, A. Rodionov, and F. Kondev, Nucl. Data Sheets **112**, 855 (2011).

[36] B. Singh, A. A. Rodionov, and Y. L. Khazov, Nucl. Data Sheets **109**, 517 (2008).

[37] E. Browne and J. Tuli, Nucl. Data Sheets **108**, 2173 (2007).

[38] P. K. Joshi, B. Singh, S. Singh, and A. K. Jain, Nucl. Data Sheets **138**, 1 (2016).

[39] N. Nica, Nucl. Data Sheets **122**, 1 (2014).

[40] E. Browne and J. Tuli, Nucl. Data Sheets **113**, 715 (2012).

[41] M. A. Cardona, G. García Bermúdez, A. Filevich, and E. Achterberg, Phys. Rev. C **42**, 591 (1990).

[42] J. Wiśniewski, W. Urban, T. Rząca-Urban, A. G. Smith, J. F. Smith, G. S. Simpson, I. Ahmad, and J. P. Greene, Phys. Rev. C **96**, 064301 (2017).

[43] W. Urban, T. Rza̧ca-Urban, A. Syntfeld-Każuch, J. L. Durell, A. G. Smith, B. J. Varley, and I. Ahmad, Phys. Rev. C **76**, 037301 (2007).

[44] S. H. Faller, J. D. Robertson, E. M. Baum, C. Chung, C. A. Stone, and W. B. Walters, Phys. Rev. C **38**, 307 (1988).